# On radar signatures of upwelling

**ALPERS Werner[1], ZENG Kan[2]**

1. *Institute of Oceanography, University of Hamburg, Hamburg, Germany*;
2. *Ocean Remote Sensing Institute, Ocean University of China, Qingdao* 266100*, China*

**Abstract:** In studies of upwelling, usually data from infrared and optical sensors are used which provide information on the Sea Surface Temperature (SST) and the Chlorophyll-a (Chl-a) concentration. In this paper, we show that also Synthetic Aperture Radars (SAR) images can give valuable contribution to such studies. Upwelling regions become detectable by SAR because they are associated with a reduction of the radar backscatter due to (1) the change of the stability of the air-sea interface (2) the presence of biogenic slicks. Furthermore, the boundary of upwelling regions consists of a line of increased radar backscatter due to the presence of convergent surface flow.

**Key words:** upwelling, synthetic aperture radar, cyclonic eddies, Agulhas Return Current, biogenic surface films, Chlorophyll concentration, air-sea interface, sea surface temperature

**Citation format: Alpers W and Zeng K. 2020. On radar signatures of upwelling. Journal of Remote Sensing(Chinese). 24(S1): 89−94**

## 1 INTRODUCTION

Upwelling in the ocean is the upward motion of water from subsurface layers resulting from horizontal divergence at the surface layer and convergence below. The most common upwelling process occurs in coastal regions in response to wind forcing parallel to the coastline, which produces a net surface water mass transport to the right of the wind direction in the Northern Hemisphere and to the left in the Southern Hemisphere due to the Coriolis force caused by the Earth's rotation (Clemente-Colon, 2014). However, upwelling can also be caused by rotational motion in cyclonic eddies (Alpers, et al., 2013) and by the interaction of currents with shallow bottom topography (like in the upwelling area north of Taiwan) (Hsu, et al, 1995). The upwelled cold water carries nutrient-rich water to the upper layers where it causes an increase of biological activity (plankton bloom). Biota in the water column always generates surface active material that ascends to the sea surface and forms there biogenic surface films or slicks that damp the small-scale surface waves that are responsible for the radar backscattering (Alpers and Espedal, 2014). Thus, the presence of biogenic surface films can serve as an indicator of biological activity as encountered massively in upwelling regions. Biogenic surface films are advected by surface currents and thus they often do not remain at the location of their generation. Furthermore, biogenic surface films often serve as tracers for eddies, which make eddies visible on Synthetic Aperture Sadar (SAR) images. The reduction of the radar backscatter or the Normalized Radar Cross Section (NRCS) caused by biogenic surface films is quite strong, usually of the order of 10 dB (Alpers and Espedal, 2014).

However, not only biogenic surface films floating on the sea surface in upwelling areas can cause a reduction of the NRCS, but also the change of the stability of the air-sea interface (from (usually) neutrally-stable to stable) because the Sea Surface Temperature (SST) is lower in upwelling areas than in the adjacent areas. Unless the difference between the air and the water temperature, $\Delta T = T_{\mathrm{air}} - T_{\mathrm{water}}$, is not extremely large, the reduction of the NRCS over upwelling areas due to the change of the stability is much smaller than by biogenic surface films, typically smaller than 3 dB (Keller, et al., 1989).

When the upwelled water reaches the sea surface, it spreads horizontally where it usually encounters stagnant waters. Thus, the flow has to decelerate, which gives rise to an area of convergence in the surface current field. Here the short surface waves, which are responsible for the radar backscatter, the so-called Bragg waves, are strained and increase their amplitude due to hydrodynamic interaction with the convergent surface current (Alpers and Hennings, 1984). According to Bragg scattering theory (Valenzuela, 1978), this causes an increase of the NRCS. Thus, upwelling areas manifest themselves on SAR images as areas of reduced NRCS values surrounded by a line of increased NRCS. However, one has to be cautious when interpreting low-value radar signatures on SAR images: Low NRCS values can also result from other effects, e. g., from coverage of the sea surface by mineral oil films or by low winds (Alpers, et al., 2017).

In the following, we present, in conjunction with other data, several SAR images acquired by the European Envisat and Sentinel-1 satellites and the Chinese Guofen-3 (GF-3) satellite that show radar signatures of upwelling caused by coastal winds, cyclonic eddies, and cyclonic meanders.

## 2 UPWELLING CAUSED BY COASTAL WINDS ALONG THE EAST COAST OF HAINAN

Hainan is a Chinese island located at the northwest corner of

**Received:** 2019-10-21; **Accepted:** 2020-04-16
**Foundation:** Ocean University of China (No. 201965003)
**First author biography:** ALPERS Werner (1936— ), male, professor. E-mail: werner.alpers@uni-hamburg.de

the South China Sea (SCS) and separated from Mainland China by the Qiongzhou Strait. During the summer monsoon, when the wind blows predominantly from a southwesterly direction, approximately parallel to the east coast of Hainan, upwelling of cold water occurs along the east coast of the island. Strong upwelling is observed when strong winds blow for few days from a southwesterly direction (Su and Pohlmann, 2009; Su, et al., 2011; Zeng, et al., 2014). Such a strong upwelling event occurred in July 2011, when a strong southwesterly wind of 10—15 m/s was blowing from 14 to 20 July along the east coast of Hainan. The southwesterly wind slackened on 21 July, and on 24 July, a light wind was blowing from the east. Remote sensing signatures of the upwelling event were captured on 24 July by the SAR onboard the Envisat satellite (spatial resolution: 30 m) via sea surface roughness variations (Fig. 1 (a)) and by the Moderate Resolution Imaging Spectroradiometer (MODIS) (spatial resolution: 1.1 km) onboard the Aqua satellite via variations of the SST and of the Chlorophyll-a (Chl-a) concentration (Fig. 2(b) and 2(c)). Fig. 1(b) shows the variation of the NRCS along a transect in the coastal area marked by a white arrow in the SAR image. The reduction of the NRCS in the dark area is up to 14 dB, which clearly indicates that the reduction is due to the damping of the Bragg waves by surface films and not by the change of the stability of the air-sea interface. Fig. 2(a) shows a band of slightly reduced SST and Fig. 2(b) a band of increased Chl-a concentration along the east coast of Hainan. Usually, with a time lag of several days, upwelling is associated with plankton bloom leading to an increase in Chl-a concentration (Fig. 2(b)) and thus to an increase in biogenic surface film coverage. Note the tongue of increased Chl-a concentration at the southeast corner of Hainan, which is associated with shallow underwater bottom topography as shown in (Su and Pohlmann, 2009). Another interesting phenomenon visible on the SAR image (Fig. 1(a)) is the curved line following the boundary of the upwelling area, which we interpret as the sea surface signature of an internal solitary wave generated by strong upwelling. Internal waves generated by upwelling have been observed on SAR images repeatedly in other upwelling areas, e.g., in the upwelling area north of Taiwan (Hsu, et al, 1995).

## 3 UPWELLING CAUSED BY A CYCLONIC EDDY OFF THE SOUTHEAST COAST OF SOUTH AFRICA

Oceanic cyclonic eddies, which are eddies in the ocean rotating counter-clockwise in the Northern Hemisphere and clockwise in the Southern Hemisphere, cause transport of cold water from lower water levels to near-surface levels. When the cold water reaches the sea surface, the stability of the air-sea interface changes from (usually) neutrally-stable to stable, which has a negative effect on the wind to generate small-scale sea surface waves. When the water is colder than the air above the sea surface, it is harder for the wind to generate short surface waves. This is because turbulence in the air layer immediately above the water surface, which is instrumental in wave generation, is reduced. Thus, the amplitude of the Bragg waves is smaller in upwelling areas than in the surrounding areas and therefore, according to Bragg scattering theory (Valenzuela, 1978), the NRCS is here lower than in the surrounding area.

An example of this phenomenon is depicted in Fig. 3(a), which shows a Sentinel-1A SAR image of a cyclonic eddy (rotating clockwise in the Southern Hemisphere). This image was acquired on 16 July 2015 at 0304 UTC in the Extra Wide (EW) swath at VV polarization in the Agulhas Current area off the southeast coast of South Africa (position of the center of the eddy: 34° S, 32° E). In the EW mode, the SAR images have a spatial resolution of 20 m x 40 m and a swath width of 410 km. Fig. 3(b) shows the geostrophic surface current streamlines as provided by the Globecurrent model (http://globcurrent. ifremer. fr/products-data/data-catalogue), which has a resolution of 1/32 deg. Fig. 3(c) shows the SST image as provided by the Odyssea Regional South Africa model (IREMER) valid for 16 July 2015. Visible is in the SAR image (Fig. 3(a)) a dark area in the lower right- hand section with a surrounding bright line. The position of this area in the SAR image matches quite well with the position of cyclonic flow pattern (Fig. 3(a)) and with the area of reduced SST values marked by an arrow in Fig. 3(c). The NRCS in the upwelling area is only slightly lower than in the surrounding area (0.5—1.5 dB), but it is surrounded by a line of increased NRCS indicating convergence of surface flow at the boundary. In this case, the reduction in NRCS cannot be due to damping of the Bragg waves due to biogenic surface films, but must be due to the change of the stability of the air-sea interface.

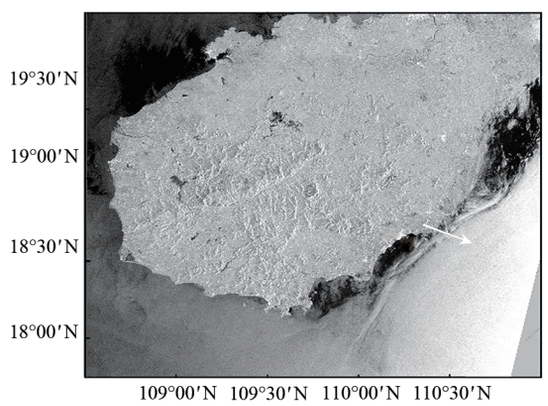


(a) Section of an Envisat SAR image (spatial resolution: 30 m) acquired on 24 July 2011 at 02:44 UTC showing part of the Chinese island of Hainan and the upwelling area off its east coast. Note the curved bright line following the boundary of the upwelling area, which, very likely, is the sea surface signature of an internal solitary wave generated by strong upwelling

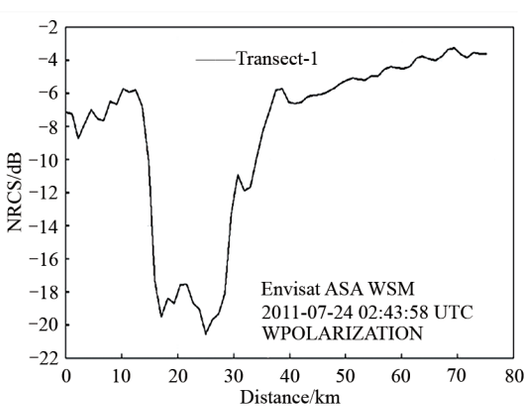


(b) Variation of the NRCS along a transect through the SAR image marked by a white arrow. Note that the reduction of the NRCS in the dark area is up to 14 dB, which clearly indicates that the reduction is due to the damping of the Bragg waves by surface films

Fig. 1

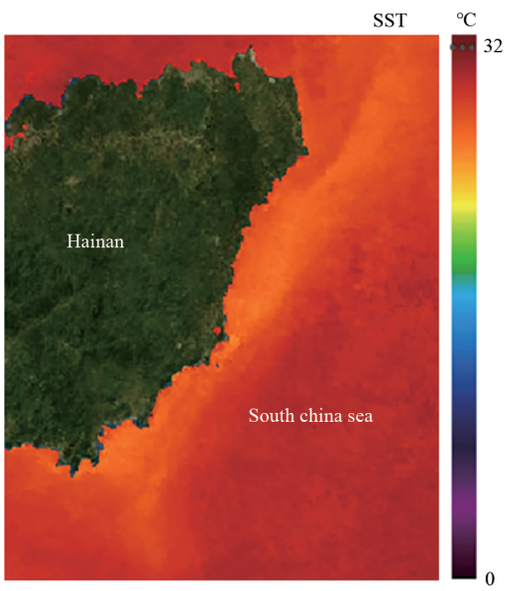


(a) SST map derived from the MODIS/Acqua data (averaged over 5 days) valid for 24 July 2011 showing a band of cold water along the east coast of Hainan

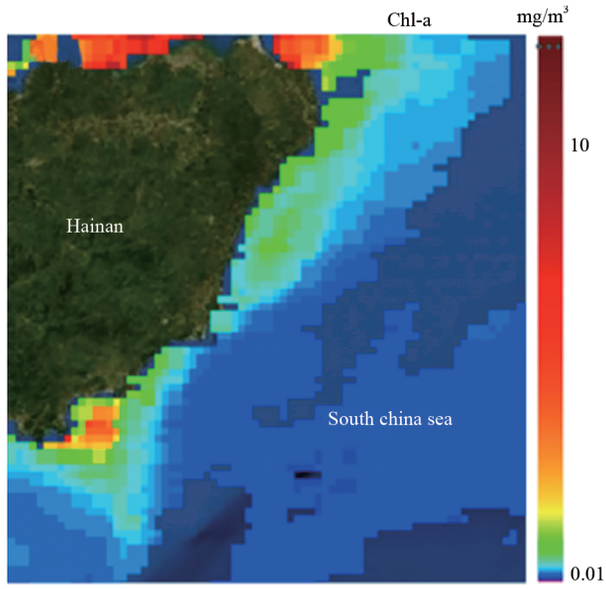


(b) Chl-a map derived from MODIS/Acqua data (averaged over 5 days) valid for 24 July 2011 showing a band of enhanced Chl-a concentration along the east coast of Hainan. Source: https//podaac-tools.jpl.nasa.gov

Fig. 2

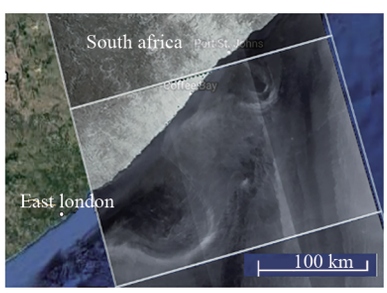


(a) Cyclonic (cold) eddy in the Agulhas Current area off the southeast coast of South Africa (position: 34° S, 32° E) imaged by Sentinel-1A on 16 July 2015 at 0304 UTC

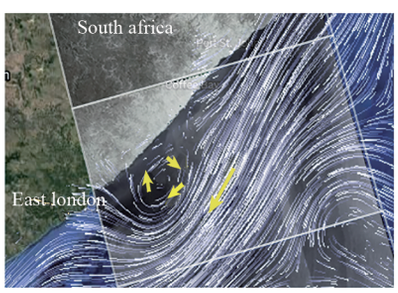


(b) Surface current field as provided by the Globecurrent model. The yellow arrows mark the direction of the surface currents

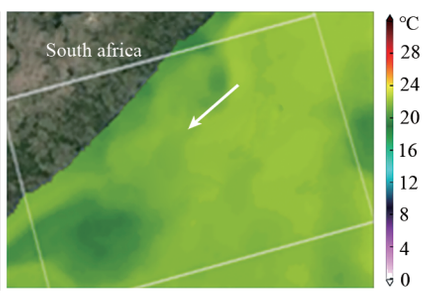


(c) Sea surface temperature (in ℃) as provided by the Odyssea Regional South Africa model (IREMER)

Fig. 3

## 4 UPWELLING AT THE WEST COAST OF SOUTH AFRICA

The upwelling at the west coast of South Africa and Namibia belongs to the Benguela upwelling system, which is one of the strongest in the world. A broad band of cold upwelled water often occurs along the west coast of South Africa (Fig. 4(b)). Often mesoscale and sub-mesoscale features, like filaments and eddies, build up at the front between the cold upwelled water and the warm surface water offshore (Flament, et al., 1985; Hoesen, et al., 2016). On the Envisat SAR image acquired on 2 May 2009 at 21: 32 UTC (Fig. 4(a)), the radar signatures of a cyclonic eddy, which has detached from the upwelling front (marked by a white broken arrow) is visible as a dark area. Since the NRCS contrast to the surrounding area is about 10 dB, the reduction can only be due to the presence of biogenic surface films associated with high biological activity. This cyclonic eddy is also visible in the SST image of 2 May 2009 (from Multi-sensor Ultra-high Resolution (MUR) SST field) produced by the Jet Propulsion Laboratory (JPL) (Fig. 4(b)) and in the Chl-a image of 5 May (derived from the MODIS/Acqua data (L3 product, 4 km resolution, averaged over 5 days) (Fig. 4(c)).

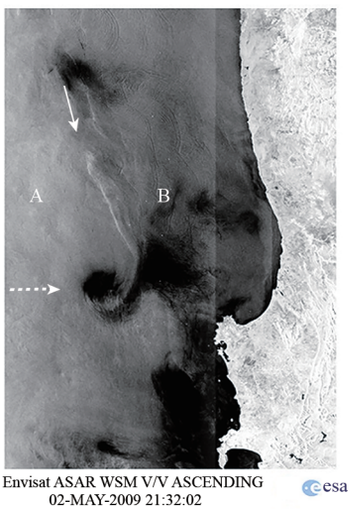


(a) Section of an Envisat SAR image acquired on 2 May 2009 at 21:32 UTC showing the upwelling area west of South Africa. The bright line (marked by a solid arrow) denotes the boundary between the upwelling cold area B and the surrounding warmer area A. Also visible is a cyclonic eddy (marked by a broken arrow)

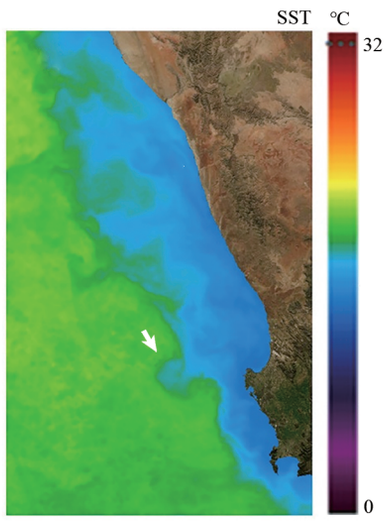


(b) SST map of 2 May 2009 showing west of the diagonal line an area of high SST values and east of it an area of lower SST values caused by cold upwelled water (marked by an arrow)

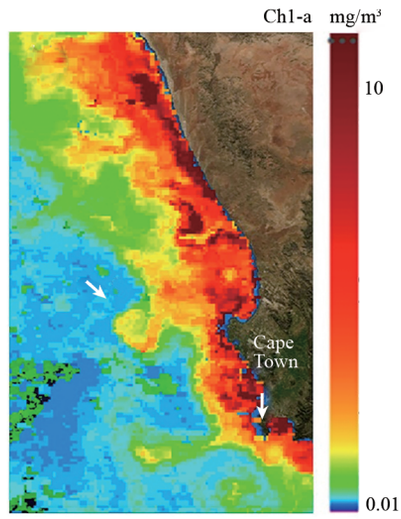


(c) Chl-a image of 5 May 2009 showing a band of enhanced Chl-a concentration along the west coast of South Africa and a cyclonic eddy (marked by an arrow). Source: https//podaac-tools.jpl.nasa.gov

Fig. 4

## 5 UPWELLING IN A MEANDER OF THE AGULHAS RETURN CURRENT

The Agulhas Current is the western boundary current of the South Indian Ocean flowing southwards along the east coast of Africa. When it reaches the southeast Atlantic Ocean, the current retroflects, i.e., it flows eastward as the Agulhas Return Current (Lutjeharms and Van Ballegooyen, 1988; Quartly and Srokosz, 1993; Boebel, et al., 2003). A schematic map of the Agulhas/Agulhas region is shown in Fig. 5. Depending on the volume transport, the location of the Return Current varies. It always exhibits a meandering pattern, which is related to the bottom topography. On 22 December 2014, a cyclonic meander (rotating clock-wise in the Southern Hemisphere) with a width of about 220 km was imaged by Sentinel-1A SAR (Fig. 6(a)) and by SST and ocean color sensors (Figs. 6(c) and 6(d)). Ocean circulation models show also a cyclonic meander at this position. Fig. 6(b) shows geostrophic surface current streamlines as provided by Globecurrent (http://globcurrent.ifremer.fr/products-data/data-catalogue [2019-10-21]). According to this model, the maximum surface current velocity is on the western side of the cyclonic meander 1.6 m/s and on the eastern side 1.4 m/s. Note that in the SAR image (Fig. 6(a)) the upwelling area is bordered by a bright line (line of increased NRCS values) indicating horizontal flow convergence. A scan through the meander pattern (not reproduced here) shows that on the western side the bright line is associated with an increase of the NRCS by 0.5 dB relative to the background and on the eastern side by an increase of 2.0 dB. A close inspection of this SAR image reveals further that inside the area bordered by the bright line another very weak bright line pattern is present indicating also here weak convergence. The SST image (Fig. 6(c)) shows low SST values inside the upwelling area and a broad band of increased SST values along the boundary, which correlates well with the broad band of increased Chl-a concentration visible in the ocean color image (Fig. 6(d)).

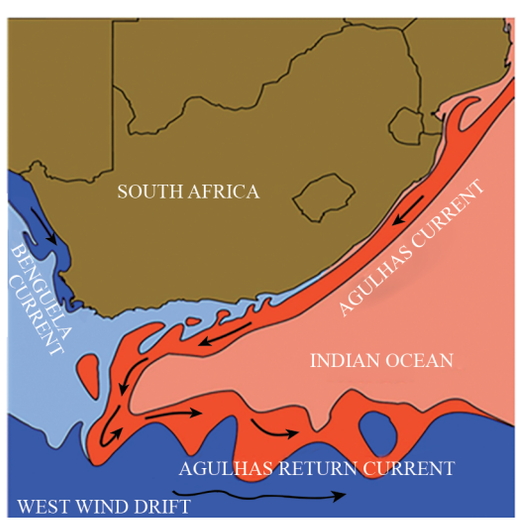


Fig. 5 Map showing the location of the Agulhas Current and the Agulhas Return Current. Red colors denote warm waters and blue colors cold waters (adopted fromhttps://en.wikipedia.org/wiki/Benguela_Current [2019-10-21])

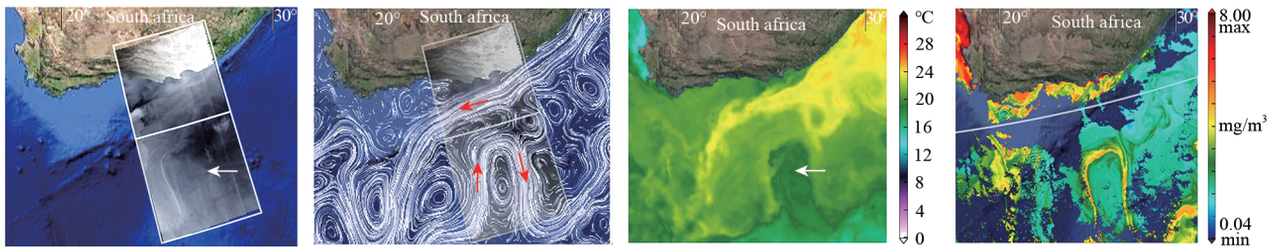


(a) South Africa (b) South Africa (c) South Africa (d) South Africa

Fig. 6 a) Sentinel-1A image acquired on 22 December 2014 at 16:50 UTC in the Extra Wide Swath Mode (swath width: 410 km) at HH polarization over the Agulhas Current/Agulhas Return Current area south of South Africa. It shows the sea surface signature of a cyclonic eddy in the Agulhas Return Current having a width of 220 km in the center (position: 7.84° S, 26.06° E). b) Geostrophic surface current streamlines on 22 December 2014 from Globecurrent. c) SST on 22 December 2014 from the Odyssea Regional Model, South Africa (IFREMER). d) Chl-a concentration on 22 December 2014 from the Visible Infrared Imaging Radiometer Suite (VIIRS) as provided by NASA.

## 6 UPWELLING ALONG THE SOUTHEAST COAST OF CHINA AND IN THE STRAIT OF TAIWAN

The east coast of China and the Strait of Taiwan are sea areas where upwelling occurs intermittently. Here upwelling is strongly controlled by bottom topography and by seasonally varying winds (Tang, et al., 2002). Fig. 6(a) shows a SAR image acquired by the Chinese GF-3 satellite on 2 September 2018 at 10:03 UTC over sections of the East China Sea and the Strait of Taiwan. It shows several dark areas (areas of strongly reduced NRCS values) in the strait and in the coastal area off Fuzhou. We interpret them as caused by damping of the Bragg waves by biogenic surface films. As stated in the Introduction, a prerequisite for the occurrence of biogenic surface films is high biological activity. Indeed, the Chl-a image derived from MODIS/Aqua data depicted in Fig. 7(b) shows increased Chl-a concentration (plankton bloom) at this time.

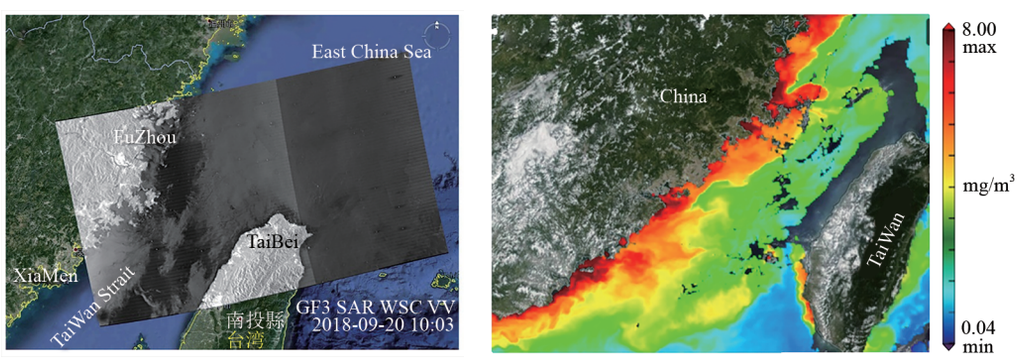


(a) (b)

Fig. 7 a) SAR image acquired by the Chinese GF-3 satellite at VV polarization on 20 September 2018 at 10:03 UTC over sections of the East China Sea and the Strait of Taiwan. It shows dark patches (areas of strongly reduced NRCS values) which, very likely, result from biogenic surface films. b) Chl-a image of 20 September 2018 derived from MODIS/Acqua data (L3 product, 4 km resolution, averaged over 5 days) showing a band of enhanced Chl-a concentration along the southeast coast of Mainland China. Source: https//podaac-tools.jpl.nasa.gov.

## 7 CONCLUSIONS

We have shown that, in addition to infrared (SST) and optical (Chl-a) images, also SAR images can provide valuable information on upwelling events. SAR has the advantage over optical instruments that it can provide images independent of cloud coverage and time of the day. Upwelling areas become visible on SAR images as areas of reduced NRCS due to the reduction of the short surface waves (Bragg waves). This reduction can be caused (1) by the change of the stability of the air-sea interface from neutrally-stable to stable due to the cold upwelled water (2) by the damping of the surface short waves by biogenic surface films produced by biota (living material) in the water column, whose concentration is usually greatly enhanced in upwelling areas. Furthermore, the boundaries of upwelling areas appear on SAR images as lines of increased NRCS values, which is due to convergent horizontal flow caused by the interaction of the upwelled water with the ambient (usually stagnant) water.

## REFERENCES

Alpers W, Brandt P, Lazar A, Dagorne D, Sow B, Faye S, Hansen W, Rubino A, Poulain P-M and Brehmer P A 2013. Small-scale oce-

anic eddy off the coast of West Africa studied by multi-sensor satellite and surface drifter data. Remote Sensing of Environment, 129:132-143, doi: 10.1016/j.rse.2012.10.032.

Alpers W, Espedal H 2014. Oils and Surfactants, Chapter 11 in Synthetic Aperture Radar Marine User's Manual, Jackson C R, Apel J R, editors, National Oceanic and Atmospheric Administration, Center for Satellite Application and Research, NOAA/NESDIS, Washington, D.C., USA, ISBN 0-16-073214-X : 263-275, available online: http://www.sarusersmanual.com.

Alpers W and Hennings I 1984. A theory of the imaging mechanism of underwater bottom topography by real and synthetic aperture radar. Journal of Geophysical Research, 89: 10529-10546.

Alpers W, Holt B and Zeng K 2017. Oil spill detection by imaging radars: Challenges and pitfalls. Remote Sensing of Environment, 20: 133-147, doi: 10.1016/j.rse.2017.09.002.

Boebel O, Rossby T, Lutjeharms J R E, Zenk W and Barron C 2003. Path and variability of the Agulhas Return Current. Deep-Sea Research, II, 50:35-56.

Clemente-Colon P 2014. Upwelling. Chapter in Synthetic Aperture Radar Marine User's Manual, Jackson C R, Apel J R, editors, National Oceanic and Atmospheric Administration, Center for Satellite Application and Research, NOAA/NESDIS , Washington, D. C., USA, ISBN 0-16-073214-X: 221-244, available online: http://www.sarusersmanual.com.

Flament P, Armi L and Washburn L 1985. The evolving structure of an upwelling filament. Journal of Geophysical Research, 90 (11): 765–11778.

Hoesen E, Moeller J, Jochumsen K and Quadfasel D 2016. Scales and properties of cold filaments in the Benguela upwelling system off Luederitz. Journal of Geophysical Research (Oceans), 121: 1896-1913, doi:10.1002/2015JC01141.

Hsu M K, Mitnik L M and Liu C T 1995. Upwelling area northeast of Taiwan on ERS-1 SAR images. Acta Oceanographica Taiwanica, 34: 27-38, doi:10.1029/2008JC005018.B.

Keller W C, Wismann V and Alpers W 1989. Tower-based measurements of the ocean C-band radar backscattering cross section. Journal of Geophysical Research, 94: 924-930, doi: 10.1029/JC094iC01p00.

Lutjeharms J R E and van Ballegooyen R C 1988. The Retroflection of the Agulhas Current. Journal of Geophysical Research, 18 (11): 1570-1583.

Quartly G D and Srokosz M A 1993. Seasonal variations in the region of the Agulhas Retroflection: Studies with Geosat and FRAM. Journal of Geophysical Research, 23: 2107-212.

Su J and Pohlmann T 2009. Wind and topography influence on an upwelling system at the eastern Hainan coast. Journal of Geophysical Research, 114, C06017.

Su J, Wang J, Pohlmann T and Xu D 2011. The influence of meteorological variation on the upwelling system off eastern Hainan during summer 2007–2008. Ocean Dynamics, 61(6): 717-730, doi: 10.1007/s10236-011-0404-9.

Tang D L, Kester D R, Ni L-H, Kawamura H, Hong H-S 2002. Upwelling in the Taiwan Strait during the Summer Monsoon detected by satellite and shipboard measurements. Remote Sensing of Environment, 83(3): 457-471, DOI: 10.1016/S0034-4257(02)00062-7.

Valenzuela G R 1978. Theories for the interaction of electromagnetic and oceanic waves-A review. Boundary Layer Meteorology, 13: 61-85.